High reflection mirrors for pulse compression gratings References and links

Stéphanie Palmier, Jérôme Neauport, N Baclet, E Lavastre, G Dupuy

High reflection mirrors for pulse compression gratings

S. Palmier,[1*] J. Neauport,[1] N. Baclet,[2] E. Lavastre,[1] G. Dupuy[1]

[1] *Commissariat à l'énergie atomique, Centre d'études scientifiques et techniques d'Aquitaine, BP2, F-33114, Le Barp, France*

[2] *Commissariat à l'énergie atomique, Laboratoire d'innovation pour les technologies des énergies nouvelles et les nanomatériaux, 17 rue des Martyrs, F-38054, Grenoble cedex, France*

**stephanie.palmier@cea.fr*

Abstract: We report an experimental investigation of high reflection mirrors used to fabricate gratings for pulse compression application at the wavelength of 1.053µm. Two kinds of mirrors are studied: the mixed Metal MultiLayer Dielectric (MMLD) mirrors which combine a gold metal layer with some e-beam evaporated dielectric bilayers on the top and the standard e-beam evaporated MultiLayer Dielectric (MLD) mirrors. Various samples were manufactured, damage tested at a pulse duration of 500fs. Damage sites were subsequently observed by means of Nomarski microscopy and white light interferometer microscopy. The comparison of the results evidences that if MMLD design can offer damage performances rather similar to MLD design, it also exhibits lower stresses; being thus an optimal mirror substrate for a pulse compression grating operating under vacuum.

OCIS codes: (140.7090) Ultrafast lasers; (050.0050) Diffraction and gratings; (350.1820) Damage; (320.2250) Femtosecond phenomena

References and links

1. N. Blanchot, G. Behar, T. Berthier, E. Bignon, F. Boubault, C. Chappuis, H. Coic, C. Damiens-Dupont, J. Ebrardt, Y. Gautheron, P. Gibert, O. Hartmann, E. Hugonnot, F. Laborde, D. Lebeaux, J. Luce, S. Montant, S. Noailles, J. Néauport, D. Raffestin, B. Remy, A. Roques, F. Sautarel, M. Sautet, C. Sauteret, and C. Rouyer, "Overview of PETAL, the multi-Petawatt project on the LIL facility," Plasma Phys. Contr. Fusion **50**(12), 124045–124055 (2008).
2. L. J. Waxer, D. N. Maywar, J. H. Kelly, T. J. Kessler, B. E. Kruschwitz, S. J. Loucks, R. L. McCrory, D. D. Meyerhofer, S. F. B. Morse, C. Stoeckl, and J. D. Zuegel, "High-energy petawatt capability for the Omega laser," Opt. Photon. News **16**, 30–36 (2005).
3. C. P. J. Barty, M. Key, J. Britten, R. Beach, G. Beer, C. Brown, S. Bryan, J. Caird, T. Carlson, J. Dawson, A. C. Erlandson, D. Fittinghoff, M. Hermann, C. Hoaglan, A. Iyer, L. Jones II, I. Jovanovic, A. Komashko, O. Landen, Z. Liao, W. Molander, S. Mitchell, E. Moses, N. Nielsen, H.-H. Ngyuen, J. Nissen, S. Payne, D. Pennington, L. Risinger, M. Rushford, K. Skulina, M. Spaeth, B. Stuart, G. Tietbohl, and B. Wattellier, "An overview of LLNL high-energy short-pulse technology for advanced radiography of laser fusion experiments," Nucl. Fusion **44**(12), S266–S275 (2004).
4. C. Le Blanc, C. Felix, J. C. Lagron, N. Forget, Ph. Hollander, M. Sautivet, C. Sauteret, F. Amiranoff, and A. Migus, "The petawatt laser glass chain at LULI: from the diode-pumped front end to the new generation of compact compressors," in Proceedings of Third International Conference on Inertial Fusion *Sciences and Applications,* B. A. Hammel, D. D. Meyerhofer, J. M. ter Vehn, and H. Azechi, eds. (American Nuclear Society) pp. 608–611 (2004).
5. C. N. Danson, P. A. Brummitt, R. J. Clarke, J. L. Collier, B. Fell, A. J. Frackiewicz, S. Hancock, S. Hawkes, C. Hernandez-Gomez, P. Holligan, M. H. R. Hutchinson, A. Kidd, W. J. Lester, I. O. Musgrave, D. Neely, D. R. Neville, P. A. Norreys, D. A. Pepler, C. J. Reason, W. Shaikh, T. B. Winstone, R. W. W. Wyatt, and B. E. Yborn, "Vulcan petawatt–an ultra-high intensity interaction facility," Nucl. Fusion **44**(12), S239–S246 (2004).
6. K. Mima, H. Azechi, Y. Johzaki, Y. Kitagawa, R. Kodama, Y. Kozaki, N. Miyanaga, K. Nagai, H. Nagatomo, M. Nakai, H. Nishimura, T. Norimatsu, H. Shiraga, K. Tanaka, Y. Izawa, Y. Nakao, and H. Sakagami, "Present status of fast ignition research and prospects of FIREX project," Fus. Sci. Technol. **47**, 662–666 (2005).
7. D. Strickland, and G. Mourou, "Compression of amplified chirped optical pulses," Opt. Commun. **56**(3), 219–221 (1985).
8. B. C. Stuart, M. D. Feit, S. Herman, A. M. Rubenchik, B. W. Shore, and M. D. Perry, "Optical ablation by high power short-pulse lasers," J. Opt. Soc. Am. B **13**(2), 459–468 (1996).

#116112 - $15.00 USD Received 24 Aug 2009; accepted 25 Sep 2009; published 23 Oct 2009

9. M. D. Perry, R. D. Boyd, J. A. Britten, B. W. Shore, C. Shannon, and L. Li, "High efficiency multilayer dielectric diffraction gratings," Opt. Lett. **20**(8), 940–942 (1995).
10. J. Keck, J. B. Oliver, T. J. Kessler, H. Huang, J. Barone, J. Hettrick, A. L. Rigatti, T. Hoover, K. L. Marshall, A. W. Schmid, A. Kozlov, and T. Z. Kosc, "Manufacture and development of multilayer diffraction gratings," in Proceedings of Laser-induced Damage Threshold in Optical Materials, G. J. Exarhos, A. H. Guenther, K. L. Lewis, D. Ristau, M.J. Soileau, C.J. Stolz, Eds, Proc. SPIE **5991**, 5991G (2006).
11. J. Neauport, E. Lavastre, G. Razé, G. Dupuy, N. Bonod, M. Balas, G. de Villele, J. Flamand, S. Kaladgew, and F. Desserouer, "Effect of electric field on laser induced damage threshold of multilayer dielectric gratings," Opt. Express **15**(19), 12508–12522 (2007).
12. P. Rambo, J. Schwarz, and I. Smith, "Development of a mirror backed volume phase grating with potential for large aperture and high damage threshold," Opt. Commun. **260**(2), 403–414 (2006).
13. J. R. Marciante, and D. H. Raguin, "High-efficiency, high-dispersion diffraction gratings based on total internal reflection," Opt. Lett. **29**(6), 542–544 (2004).
14. T. Clausnitzer, J. Limpert, K. Zöllner, H. Zellmer, H. J. Fuchs, E. B. Kley, A. Tünnermann, M. Jupé, and D. Ristau, "Highly efficient transmission gratings in fused silica for chirped-pulse amplification systems," Appl. Opt. **42**(34), 6934–6938 (2003).
15. C. Stolz, J. R. Taylor, W. K. Eickelberg, and J. D. Lindh, "Effects of vacuum exposure on stress and spectral shift of high reflective coatings," Appl. Opt. **32**(28), 5666–5672 (1993).
16. H. Leplan, "Les contraintes dans les couches minces optiques", PhD Thesis (1995).
17. R. Thielsch, A. Gatto, and N. Kaiser, "Mechanical stress and thermal-elastic properties of oxide coatings for use in the deep-ultraviolet spectral region," Appl. Opt. **41**(16), 3211–3217 (2002).
18. D. Smith, M. McCullough, C. Smith, T. Mikami, and T. Jitsuno, "Low stress ion-assisted coatings on fused silica substrates for large aperture laser pulse compression coatings," in Proceedings of Laser-Induced Damage in Optical Materials: 2008, G. J. Exarhos, D. Ristau, M. J. Soileau, C. J. Stolz Eds, Proc. SPIE **7132**, 71320E (2008).
19. N. Bonod, and J. Neauport, "Optical performances and laser induced damage threshold improvement of diffraction gratings used as compressors in ultra high intensity lasers," Opt. Commun. **260**(2), 649–655 (2006).
20. N. Blanchot, G. Marre, J. Néauport, E. Sibé, C. Rouyer, S. Montant, A. Cotel, C. Le Blanc, and C. Sauteret, "Synthetic aperture compression scheme for a multipetawatt high-energy laser," Appl. Opt. **45**(23), 6013–6021 (2006).
21. J. B. Oliver, T. J. Kessler, H. Huang, J. Keck, A. L. Rigatti, A. W. Schmid, A. Kozlov, and T. Z. Kosc, "Thin-film design for multilayer diffraction gratings, " in Proceedings of Laser-induced Damage Threshold in Optical Materials, G. J. Exarhos, A. H. Guenther, K. L. Lewis, D. Ristau, M.J. Soileau, C. J. Stolz, Eds, Proc. SPIE 5991 (2006).
22. S. Liu, J. Ma, Z. Shen, Y. Jin, J. Shao, and Z. Fan, "Optimization of thin-film design for multi-layer dielectric gratings," Appl. Surf. Sci. **253**(7), 3642–3648 (2007).
23. http://www.optilayer.com
24. J. Y. Robic, H. Leplan, Y. Pauleau, and B. Rafin, "Residual stress in silicon dioxide thin films produced by ion-assisted deposition," Thin Solid Films **290**, 34–39 (1996).
25. G. Théret, "Les couches minces de HfO2. Etude de leurs hétérogénéités d'indice de réfraction et de leur interface avec SiO2," PhD Thesis, (2001).
26. B. C. Stuart, M. D. Feit, A. M. Rubenchik, B. W. Shore, and M. D. Perry, "Laser-induced damage in dielectrics with nanosecond to subpicosecond pulses," Phys. Rev. Lett. **74**(12), 2248–2251 (1995).
27. M. Mero, J. Liu, W. Rudolph, D. Ristau, and K. Starke, "Scaling laws of femtosecond laser pulse induced breakdown in oxide films," Phys. Rev. B **71**(11), 115109 (2005).
28. TFCalc, Software Spectra Inc., Portland, OR, USA, *www.sci-soft.com*
29. M. Birnbaum, "Semiconductor surface damage produced by ruby lasers," J. Appl. Phys. **36**(11), 3688 (1965).
30. J. F. Young, J. S. Preston, H. M. van Driel, and J. E. Sipe, "Laser-induced periodic surface structure. II. Experiments on Ge, Si, Al, and brass," Phys. Rev. B **27**(2), 1155–1172 (1983).
31. T. Z. Kosc, A. A. Kozlov, and A. W. Schmid, "Formation of periodic microstructures on multilayer dielectric gratings prior to total ablation," Opt. Express **14**(22), 10921–10929 (2006).
32. D. C. Emmony, R. P. Howson, and L. J. Willis, "Laser mirror damage in germanium at 10.6μm," Appl. Phys. Lett. **23**(11), 598 (1973).
33. A. Brenner, and S. Senderoff, "Calculation of stress in electrodeposits from the curvature of a plated strip," J. Res. Natl. Bur. Stand. **42**, 105–123 (1949).
34. A. E. Ennos, "Stresses developed in optical film coating," Appl. Opt. **5**(1), 51 (1966).
35. H. P. Murbach, and H. Wilman, "The origin of stress in metal layers condensed from the vapour in high vacuum," Proc. Phys. Soc. **66B**, 905 (1953).

1. Introduction

The past decade has seen the development of numerous large laser facilities offering ultra high intensity beams with hundred joules to multi-kJ capabilities [1–6]. These systems use the chirped pulse amplification technique introduced in 1985 [7]. In this context, grating has been the object of major improvements in order to withstand always higher laser fluences in short pulse regime and also to exhibit high diffraction efficiency. First gratings used were gold

#116112 - $15.00 USD Received 24 Aug 2009; accepted 25 Sep 2009; published 23 Oct 2009

relief gratings. But their rather limited diffraction efficiency (90% to 94%) and damage threshold of about 0.5 J/cm^2 beam normal for picosecond pulses at the wavelength of 1.053µm induced by the gold layer itself [8] pushed developments to new extends. MultiLayer Dielectric (MLD) grating concept was proposed by Perry in 1995 [9]. Consisting of a grating engraved on the top layer of a MLD mirror, this new design offers better diffraction efficiency (>95%) and improved damage performances mainly limited by the quality of deposited dielectric layers and geometry of the grating structure. Typical thresholds of some J/cm^2 can be reached in picosecond regime depending on the grating type in terms of line density and incidence [3, 9–11]. Various alternative solutions were also studied such as volume phase gratings [12], total internal reflection gratings [13] or transmission gratings [14]. Nevertheless, none was really retained for petawatt class laser facilities probably due to nonlinear effects concerns for transmissive gratings and environment sensitivity for phase holograms. Hence, efforts are still made to enhance MLD grating performances.

Pulse compression gratings operate under high-vacuum environment. Dielectric coatings used for the mirror of the MLD gratings are composed of alternative layers of low index and high index oxides (usually HfO_2 and SiO_2). This MLD coating induces stresses between the substrate and the coating that can distort the wavefront [15, 6] and in catastrophic cases causes crazing (see Fig. 1). Moreover the porous structure of oxide layers makes them sensitive to environment conditions; consequently stress is likely to be modified when changing from air to vacuum.

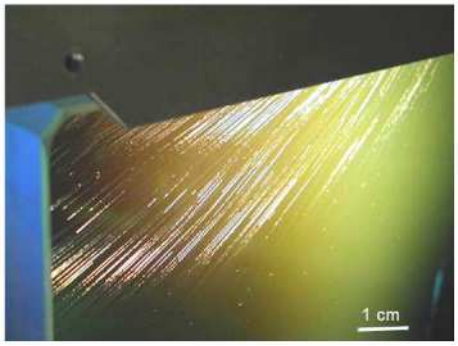

Fig. 1. Typical case of crazing observed on an HfO_2/SiO_2 high reflection e-beam evaporated mirror.

Managing stress and vacuum sensitivity of MLD coating has thus become an important issue for MLD grating manufacturers. A first solution to minimize this effect is to use Ion Assisted deposition technique (IAD) instead of e-beam evaporation. IAD has been demonstrated to able to produce dense layers with no water absorption on both mono-layers and high reflection mirrors [17] and more recently on MLD gratings [18]. A different option is to minimize the coating thickness. We studied in a previous work the feasibility of mixed Metal MultiLayer Dielectric (MMLD) grating; a gold layer is inserted between the substrate and some e-beam evaporated pairs of HfO_2/SiO_2 to constitute a mirror under the low index top layer of which the a grating is engraved [19]. We evidenced that this design is compatible with a high efficiency in the diffracted order and a low electric field enhancement inside the grating pillar i.e. potential high damage resistance under short pulse irradiation [11].

In this paper, we report on an experimental investigation of MMLD mirrors designed to be engraved to become MMLD gratings. A comparison between MLD and MMLD is also carried out. Mirror thin film design is done so that the mirror can be used to make a high efficiency and high damage threshold 1780 l/mm pulse compression grating, operating at 77.2°, TE polarization, i.e. PETAL grating vacuum compressor specifications [20]. We detail samples manufacturing in section 2 with some details on stack design, coating deposition process and metrology. Section 3 is devoted to the description of the different characterization

#116112 - $15.00 USD Received 24 Aug 2009; accepted 25 Sep 2009; published 23 Oct 2009

methods used: damage testing, Nomarski microscopy and WLI. Results are discussed in section 4; finally we offer our conclusions in the last section.

2. Experimental procedure

2.1. Stack design

Two kinds of grating support mirrors are studied: the MLD mirror and the MMLD mirror. Both designs are engineered to cope with various specifications [21, 22]. In peculiar, the mirror shall exhibit a high reflectivity for $(0)^{th}$ and the $(-1)^{th}$ order of the 1780l/mm grating [19], thus being centered at the median angle of these two angles. Hence it must have a reflectivity of more than 99% at 1.053µm for an incidence of 70.6° under vacuum. Regarding the specific case of the MMLD, we also need to reduce the amount of energy coming to the gold interface to ensure high damage performances while maintaining a sufficient number of manufacturable grating solutions at the end. We demonstrated in a previous work that 4 pairs of HfO_2/SiO_2 were a good trade off [19]. Finally, the low index overcoat thickness that shall receive the grating is chosen with the same consideration i.e. ensure a high diffraction efficiency for the final compression grating with large manufacturing tolerances [19]. The selected designs are the following ones:

MLD: Pyrex / $(115nm\ HfO_2\ 311nm\ SiO_2)^8$ $115nm\ HfO_2$ $385nm\ SiO_2$

MMLD: Pyrex / 20nm Cr 150nm Au $(246nm\ SiO_2\ 155nm\ HfO_2)^4$ $579nm\ SiO_2$

The refractive index of the SiO_2 and HfO_2 materials that were used in the simulation were measured on the monolayers deposited by EBPVD (See section below).

2.2. Sample preparation methods

All the multilayers were manufactured on Pyrex substrates (50-mm diameter, 5-mm thickness), by Electron Beam Physical Vapour Deposition (EBPVD). For the MMLD mirrors, the chromium (20 nm) and gold (150 nm) layers were deposited at room temperature with a deposition rate of $0.8nm.s^{-1}$ and $0.4nm.s^{-1}$ respectively. For the MLD and MMLD multilayers, the SiO_2 dielectric layer was deposited from a SiO_2 source with a deposition rate of $0.47nm.s^{-1}$. The HfO_2 dielectric layer was deposited from a metallic Hf source, under an oxygen partial pressure of 3.10^{-4}mbar at a temperature of 125°C; the deposition rate was $0.3nm.s^{-1}$.

First SiO_2 and HfO_2 monolayers were manufactured in order to characterize their optical properties and to check the thickness homogeneity on the whole substrate surface. Optical characterization (reflectivity and transmittance) was performed with a Perkin-Elmer spectrophotometer in the 300-2600nm range. The refractive indexes were then obtained from Optilayer simulations [23]: at 1053nm, 1.45 for SiO_2 and 1.92 for HfO_2. The thickness of both monolayers was measured by a mechanical profilometer and confirmed from spectrophotometry measurements and Optilayer calculations. The relative thickness uniformity on the whole surface of the substrates was around 0.6% and 0.9% for SiO_2 and HfO_2 layers, respectively. For the SiO_2 layer, the density was calculated from the refractive index measured at 600nm, following a method proposed by Robic [24]; a density of $1.88g.cm^{-3}$ was then obtained. The Bruggeman law allowed determining the density of the HfO_2 monolayer from the refractive index measured at 500nm [25]; a density of $7.94g.cm^{-3}$ was obtained.

Then, the two mirror designs previously described were deposited in the same conditions as for the SiO_2 and HfO_2 monolayers. For each design, the reflectivity was measured on the 300-2600nm range and is shown on Fig. 2.

#116112 - $15.00 USD Received 24 Aug 2009; accepted 25 Sep 2009; published 23 Oct 2009

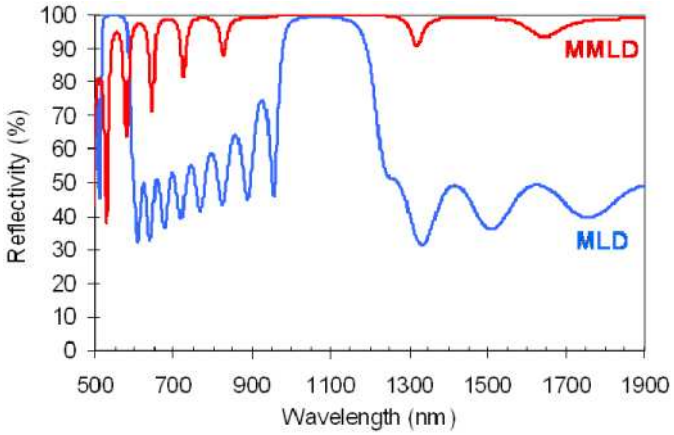

Fig. 2. Reflectivity of the MLD and MMLD designs measured for an incident angle of 70.6° and a TE polarization.

The TE-polarized reflectivity at 1053 nm is 99.41% and 99.96% for the thin MLD and MMLD multilayers, respectively for an incidence of 70.6°. For both designs, the reflectivity remains rather constant around 1053 nm particularly for the MMLD which reveals the "robustness" of the developed design. Thicknesses of the various layers were then optimized to fit the measured curves; final stacks designs after this fitting are shown in Table 1.

Table 1. Nominal and fitted designs for each kind of samples.

	Nominal design	**Fitted design**
MLD	Pyrex / (115nm HfO_2 311nm SiO_2)^8 115nm HfO_2 385nm SiO_2	Pyrex / (94nm HfO_2 352nm SiO_2)^8 94nm HfO_2 434nm SiO_2
MMLD	Pyrex / 20nm Cr 150nm Au (246nmSiO_2 155 nmHfO_2)^4 579nm SiO_2	Pyrex / 20nm Cr 150nm Au (232nm SiO_2 157nm HfO_2)^4 574nm SiO_2

2.3. Sample characterization methods

To study laser damage resistance, an experimental set up called DERIC was developed at the CEA/CESTA. All the details of this set up can be found elsewhere [11]. The main parameters are recalled below. DERIC is characterized by a Gaussian laser beam with wavelength of 1057 nm, pulse duration of 500 fs, a diameter of 200 µm at $1/e^2$ on the sample. The repetition rate is 10 Hz. Fluences are always given in beam normal with a precision of +/– 9%. Damages are detected by the operator thanks to a long working distance microscope equipped with CCD camera (resolution of about 10µm). Tests are performed at a temperature of 20°C under dry air (RH<10%).

The test mode is S on 1. Depending on the sample behaviour during the damage test, from 20 to 50 sites are exposed to a burst of 100 laser pulses at a specified fluence. This operation is repeated for different fluences. Then each damage site is counted in order to get a damage probability for each fluence. From theses results, the laser induced damage threshold (LIDT) i.e. the highest fluence value for which no damage is detected, is determined. For operating considerations, two incidences where used during MMLD and MLD samples characterizations; MMLD mirrors were tested at 72° and MLD at 77.2° both in TE-polarization. It must be outline that the mirror stack designs ensure a high reflexion of more than 99% at both angles as depicted in Fig. 3. Before testing, samples were cleaned by a drag wipe method with ethanol. Damages are then observed by Nomarski microscopy. Some of them are observed with a White Light Interferometer (WLI).

#116112 - $15.00 USD Received 24 Aug 2009; accepted 25 Sep 2009; published 23 Oct 2009

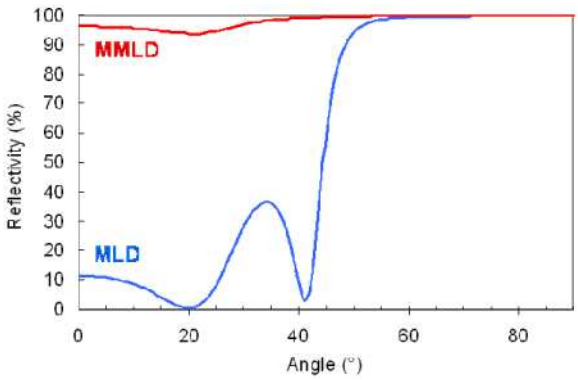

Fig. 3. Reflectivity of the MLD and MMLD designs simulated at 1.053µm in a range of incidence from 0° to 90°.

3. Results and discussions

3.1 Laser damage

Four samples (2 MMLD and 2 MLD) were tested on the DERIC set up in the conditions detailed above. The probability curve obtained for each sample is showed in Fig. 4. Squares represent the results obtained for the MLD and the triangles for the MMLD. Lines are added to guide the eyes.

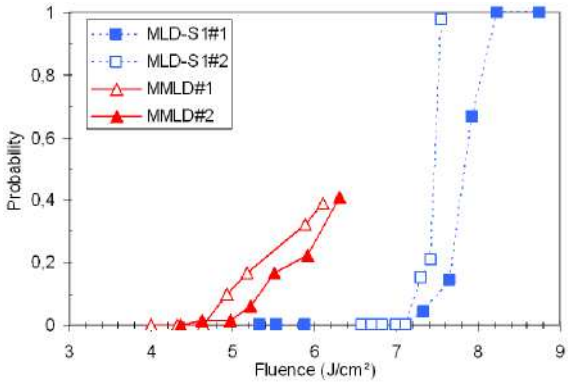

Fig. 4. Damage probability curves obtained after laser irradiation of different samples at 1057nm, 500fs, TE polarization. MLD are tested at an incidence of 77.2°, MMLD are tested at 72°. No angular correction is made.

The two samples of the same kind show the same tendency. The MMLD LIDT is of about 4.4 J/cm^2 at an incidence of 72°. The MLD LIDT is of about 7J/cm^2 at an incidence of 77.2°. If an angular projection is made, it corresponds to a LIDT of 5J/cm^2 which is rather similar to the MMLD performances. Consequently the gold layer does not reduce the stack LIDT. The noticeable difference between MMLD and MLD is the curve slope. A low slope such as the MMLD one is preferable for laser applications.

Usually, classical λ/4 stacks are weakened by the low damage threshold of material such as Au or HfO_2. In short pulse regime, damage is dominated by collisional and multiphoton ionization and plasma formation [26]. So it is strongly dependent of the electric field intensity. Damage occurs when the local electric field intensity of the laser beam reaches a critical value in the stack [27]. Theoretical Electric Field Intensities (EFI) were therefore calculated by using a commercial software for thin film optical design and analysis TFCalc [28]. Figure 5 illustrates the electric field distribution in the stack of the MLD (Fig. 5(a)) and the MMLD (Fig. 5(b)) as a function of distance measured normal to the surface of the layers for radiation incident from the left.

#116112 - $15.00 USD Received 24 Aug 2009; accepted 25 Sep 2009; published 23 Oct 2009

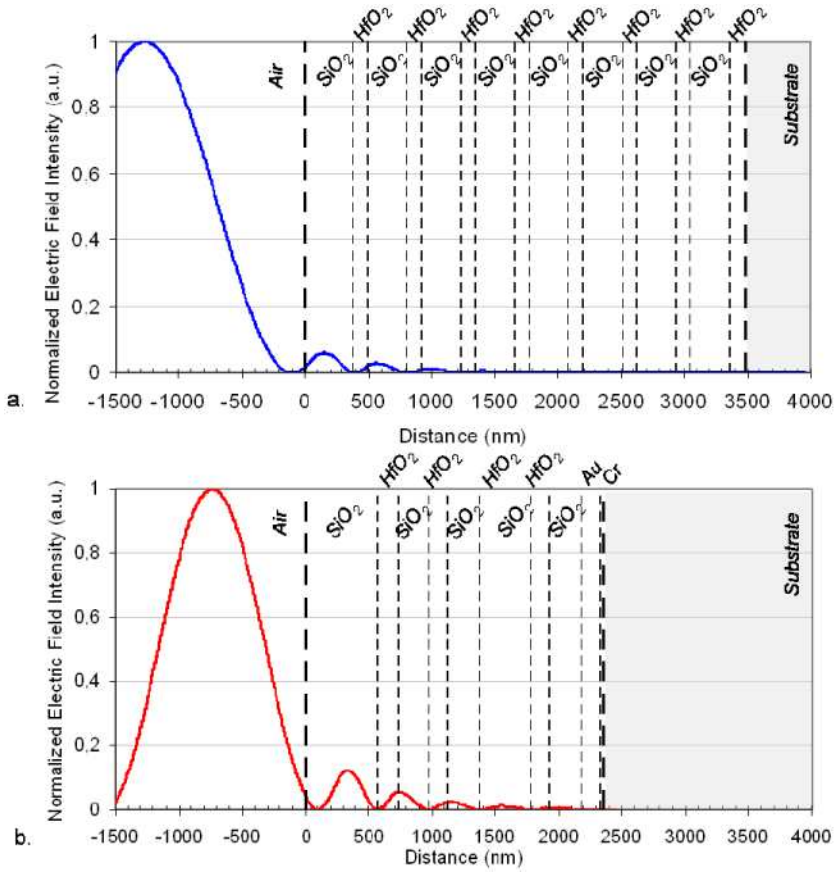

Fig. 5. Electric field distribution of the MLD (a) and the MMLD (b) samples. EFI is calculated and plotted in the damage testing conditions i.e. 72° for the MMLD and 77.2° for the MLD.

In Fig. 5(a) and (b), the EFI is seen to vary from minimum to maximum values in silica layers. The minimum occurs at the interfaces between SiO_2 and HfO_2 and the maximum in SiO_2 layers or next to the HfO_2/SiO_2 interface. Little by little, the EFI decreases in the stack to be equal to zero in the layer in contact with the substrate. The EFI equals to zero in the gold layer (Fig. 5(b)) evidences that damage is not initiated by this low damage resistant material. The peak field occurs in the SiO_2 overcoat and its intensity is about 0.06 for the MLD mirror; while the EFI is still 0.13 in the case of the MMLD mirror. The ratio of these maximum EFI between MMLD and MLD is in the same range as measured LIDT with a factor of about 2. According to these results, the peak field and hence the damage should occur in the SiO_2 overcoat. This is confirmed by the analysis of the damage morphology. After the laser damage resistance test, damages are observed by Nomarski microscopy. All the observed damages result in a 100-shots illumination. Figure 6 shows typical damages seen on MLD and MMLD samples.

#116112 - $15.00 USD Received 24 Aug 2009; accepted 25 Sep 2009; published 23 Oct 2009

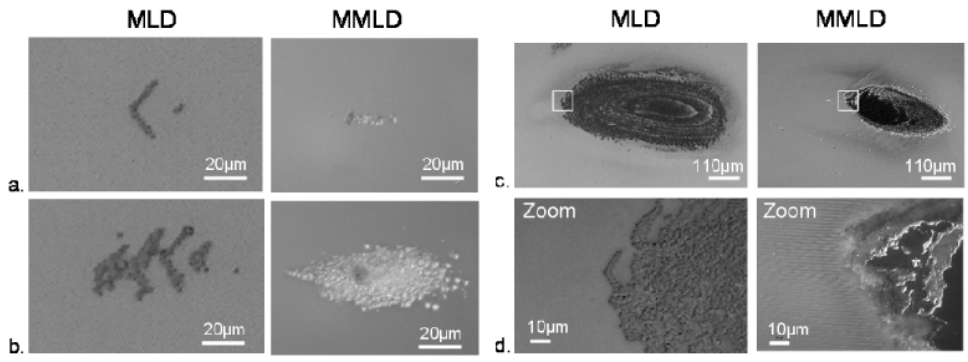

Fig. 6. Damage morphology of MLD samples (left) and a MMLD samples (right) at different stage of the damage: the initiation (Fig. 6(a)), the growth (Fig. 6(b)) and the final damage obtained at the highest fluence (Fig. 6(c)). Figure 6(d) is a zoom of the Fig. 6(c) white square.

In both cases, damage initiation (Fig. 6(a)) is superficial. This confirms that damage appears in the SiO_2 overcoat where the EFI is the most important. But damage morphology differs from the two kinds of samples. On most of MLD damages, a typical arrow shape structure is observed. On MMLD, damages more look like pits. At higher fluence (Fig. 6(b)), the number of arrows on the MLD and pits on the MMLD is more important. On both samples, damage tends to be more expanded then deep. This effect is also seen on Fig. 6(c), at a high fluence, the length is limited by the laser spot size but not its depth. Damage results in a rapid plasma formation and surface ablation and so it is limited to the region where the laser fluence is sufficient [26]. An interesting aspect can also be seen on Fig. 6(d): a structure is printed all around the damages. It always appears perpendicularly to the beam polarization and with a roughly constant period. This grating like-structure called ripples was further explored by WLI. Figure 7 illustrates the observations on both samples.

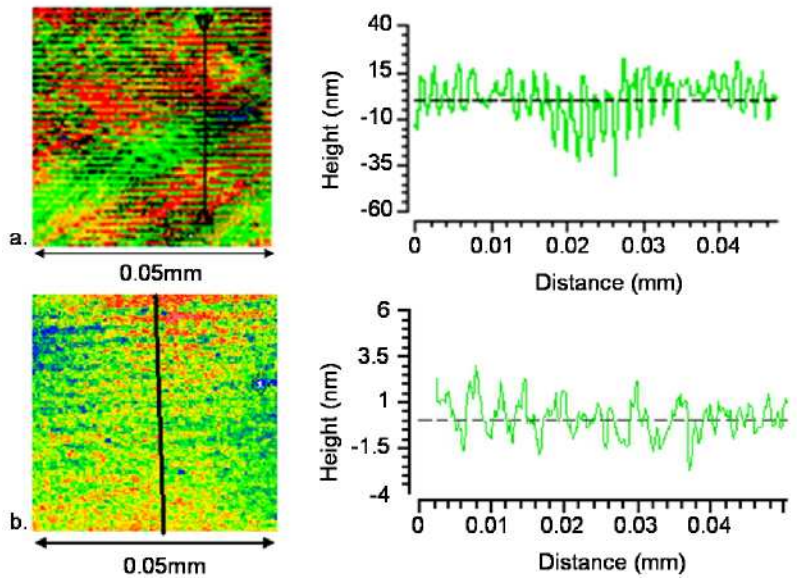

Fig. 7. Ripples cartography (on the left) and profile (on the right) on a MMLD sample (a) and a MLD sample (b) irradiated at high fluence.

Figure 7(a) shows that ripples are engraved in the SiO_2 overcoat. It is a kind of grating with a period of about 1500nm. The depth of these ripples varies from 5 to 20nm (peak to

#116112 - $15.00 USD Received 24 Aug 2009; accepted 25 Sep 2009; published 23 Oct 2009

valley). Figure 7(b) shows that even if it is not observable by Nomarski microscopy, ripples are also present on the MLD samples. They are less distinct and less deep, about 5nm (peak to valley), with a similar period. Ripples were first observed on various semiconductor surfaces by Birnbaum [29]; they can also appear and metal [30]. If in the latter, they are associated with the creation of a surface plasmon during laser interaction, their origin is less understood in the case of dielectrics and various explanations are still under debate. In the field of short pulse optical components, ripples were already observed on MLD grating [11, 31], we herein see that they can also be seen on mirrors. Emmony studied the effect of incidence on ripples period and evidenced that ripples period p is related to the incidence angle θ and to the wavelength λ by the relation $p=\lambda/(1-\cos\theta)$ (in this relation, the incidence angle is defined by the angle between the normal to the sample surface and the laser beam propagation axis) [32]. The period measured on both samples fulfils this relation.

3.2 Stresses

Mirrors for pulse compression gratings have to withstand a high energy and tough environment. To work properly under vacuum and despite the air/vacuum cycles, stacks have to be engineered in order to get a very low residual stress and thus to avoid substrate power or crazing. Hence, residual stress of manufactured samples was analysed. For our samples, the Pyrex substrate thickness (5mm) is much more important than the coating thickness (<3µm). From the mechanical point of view, each layer of the stack interacts independently and directly on the substrate [16]. The final power of the substrate is a linear superposition of the deflection induced by each layer of the stack. Total residual stress in the stack can then be obtained from measurements performed on SiO_2 and HfO_2 monolayers. For a substrate (denominated S) with a length L, a thickness t_s and coated by N layers with a thickness t_i and a stress σ_i, the power variation is given by Eq. (1):

$$\Delta f = \frac{3}{4}\frac{1-\nu_s}{E_s}\frac{L^2}{t_S^2}\sum_{i=1}^{N}\sigma_i.t_i \tag{1}$$

where E_s and ν_s are Young's modulus and Poisson's ratio of the substrate. The total stress for each monolayer is the sum of several contributions: the intrinsic stress that is directly linked to the coating deposition, the thermal stress that appears during the cooling of the coating (if the latter is not performed at room temperature), and the environmental stress that depends on the environment of the coating: air, vacuum… The total stress of the SiO_2 and HfO_2 layers deposited on silicon substrate by EBPVD in similar conditions (same high vacuum evaporation equipments, temperature, and oxygen partial pressure) was taken from a previous work of Leplan [16]. The main difference between these measurements and our sample is the substrate: the single SiO_2 and HfO_2 films were deposited on (111)-oriented single crystal Si substrates. Only the thermal stress depends on the nature of the substrate. To evaluate the residual stress of these thin SiO_2 and HfO_2 films deposited on Pyrex substrate, the Eq. (2) is used:

$$\sigma_{pyrex} = \sigma_{silicon} - \sigma_{silicon}^{thermal} + \sigma_{pyrex}^{thermal} \tag{2}$$

and the thermal stress can be expressed as in Eq. (3) [33]:

$$\sigma^{thermal} = \left(\frac{E}{1-\nu}\right)_{coating}(\alpha_{substrate} - \alpha_{film}).\Delta T \tag{3}$$

where $\alpha_{substrate}$ and α_{film} are the thermal expansion coefficients of the substrate and the film and ΔT is the temperature difference between the ambient and the coating temperature; in the present case, $\Delta T = 105°C$. According to Leplan results, total residual stress in SiO_2 films deposited on silicon substrate was −86MPa (a negative value corresponds to a compressive stress) and in HfO_2 films was +66MPa. Using Eq. (2) and (3), the residual stress obtained for

#116112 - $15.00 USD Received 24 Aug 2009; accepted 25 Sep 2009; published 23 Oct 2009

the SiO_2 and HfO_2 monolayers on a Pyrex substrate are respectively −92MPa and +49MPa. For the chromium and gold monolayers, the residual stress is respectively +128MPa [34] and +83MPa [35]. We estimated the deformation induced by the coating for a full scale 450×420×43mm^3 pulse compression grating by using Eq. (1) with a biaxial modulus of Pyrex equal to $E_S/(1-\nu_S)$=80GPa. Calculated powers are given in Table 2.

Table 2. Power of the Pyrex substrate induced by the different stacks.

	MLD	MMLD
Total stress (Mpa)	−63	−40
Power calculated for a full scale PETAL pulse compression grating (nm)	−264 λ/4	−95 λ/11

Although the total stress for both designs is comparable, it has a strong influence on the power on a full scale component. This coating induced deformation can be reduced with a factor 8 by using a MMLD design.

4. Conclusion

An experimental study was carried out to compare classical MLD mirror and a new stack design called MMLD in which a gold layer is inserted to replace a few pairs of HfO_2/SiO_2. Both kinds of samples were silica overcoated in order to allow the grating etching. The damage resistance tests results show that the MMLD LIDT is comparable with the MLD and in good concordance with EFI values. Analysis of damage morphology revealed that damage occurs in the silica overcoat. Ripples are also observed all around damage sites. To go further on the study of these samples, the residual stress and the power induced by each kind of stacks was evaluated for full scale PETAL pulse compression grating. It was found that the MMLD coating is less stressed than MLD. From these results, we demonstrate that MMLD mirrors for pulse grating application are a good trade off.

Acknowledgments

This work is being performed under the auspices of the Conseil Régional d'Aquitaine, of the French Ministry of Research and of the European Union and with the technical supports of the Institut Lasers et Plasmas. DERIC damage testing facility development was performed under the auspices of Laserlab-Europe program. We thank the ALISÉ team for access to and modular capabilities of ALISÉ facility, Christophe Leymarie for the WLI measurements, and N. Bonod (Fresnel Institut) for pulse compression grating numerical optimization.